Lattice vibrations of $AgGaS_2$, $AgGaSe_2$, and $CuGaS_2$

J. P. van der Ziel, A. E. Meixner, H. M. Kasper, and J. A. Ditzenberger
Bell Laboratories, Murray Hill, New Jersey 07974
(Received 29 November 1973)

Raman spectra have been observed in $AgGaS_2$, $AgGaSe_2$, and $CuGaS_2$ using argon, krypton, and dye lasers. Of the 13 Raman-active vibrations, we have observed 12 of the modes of $AgGaS_2$, 9 modes of $AgGaSe_2$, and all the modes of $CuGaS_2$. The modes of $AgGaS_2$ which are also infrared active are in good agreement with the modes determined from a Kramers-Kronig analysis of the ir reflectivity. Agreement is also found with several of the transitions previously determined from the ir spectrum of $CuGaS_2$. The intensity of the A_1 mode of $AgGaS_2$ and $CuGaS_2$ dominates the other Raman lines when the laser excitation is well below the band gap. A resonant interference effect decreases the intensity of this mode as the band gap is approached.

I. INTRODUCTION

The $A^{I}B^{III}C_2^{VI}$ compounds are ternary semiconductors which have the chalcopyrite structure and belong to the D_{2d}^{12}–$I\bar{4}2d$ space group.[1,2] The physical properties of the chalcopyrites are in general quite similar to the binary $A^{II}B^{VI}$ analogs which have the cubic zinc-blende structure.[3] However, the presence of the third atomic component as well as the noncubic structure increases the possible range of application. Thus, $AgGaS_2$ is of interest as a nonlinear material because it has a direct band gap[3] in the blue at 2.75 eV, a large nonlinear optical coefficient,[4,5] and sufficient negative birefringence to allow phase-matched optical harmonic generation. The selenide has a 1.65-eV direct band gap[6] and is useful for nonlinear optical phase matching relatively further in the infrared.[7] The semiconducting properties of $CuGaS_2$, with its 2.4-eV direct band gap, are of interest.[8] The optical and electrical properties of these materials have also been studied.[9–11]

We have studied the phonon modes of these materials by Raman scattering. Inspired to look for the relationships between the vibrations of $AgGaS_2$ and the II-VI compounds, one of us (J. A. D.) studied the ir-active modes of $AgGaS_2$, and the results obtained are given in Sec. III C. These ir-active modes are in good agreement with our Raman data. However, the energies and the assignments differ somewhat from the results of a later Raman and infrared study.[12] Most of the ir-active modes of $CuGaS_2$ are known from an analysis of the reflectivity,[13] and several of these modes are in reasonable agreement with Raman spectra reported here. The availability of data on a number of crystals enables us to compare the effects of anion and cation mass on the phonon spectrum, and this is discussed in Sec. IV.

For the sulfides a major fraction of the total Raman scattering intensity is contained in the single A_1 mode when the laser excitation energy is well below the band gap. However, the A_1 intensity is found to decrease, and become of the same order as the other modes, as the excitation energy approaches the band gap. This resonance interference effect is discussed in Sec. III D.

II. CRYSTAL SYMMETRY AND LATTICE VIBRATIONS

The body-centered-tetragonal unit cell shown in Fig. 1 contains four formula units.[1] There are a total of 24 modes of vibration whose transformational properties are characterized by the irreducible representations given in Table I.[14]

The Raman-active A_1 mode was detected in the $x(zz)\bar{x}$ and $x(yy)\bar{x}$ backscattering geometries and the B_1 mode was observed in the latter geometry. The B_2 and E modes are infrared as well as Raman active, and since these modes may have a finite dipole moment, it is necessary to distinguish between the longitudinal (L) and transverse (T) components in the Raman spectrum. This requires the proper selection of the direction of propagation as well as the polarization of the phonons.[15] In the backscattering configuration the B_{2z}(L) mode appears in the $z(xy)\bar{z}$ geometry, and the E_x(L) mode appears in the $x(zy)\bar{x}$ geometry. The B_{2z}(T) and E_x(T) modes were isolated in the 90° $x(yx)y$ and $y(zy)z$ geometries, respectively, as well as in the approximate forward-scattering geometries $\tilde{z}(yx)z$ and $\tilde{y}(zx)y$. The direction of laser propagation, as denoted by the tildes, was adjusted to be slightly away from the z or y axis and have a small x component. The noncolinearity of the incident and scattered waves yields a scattered phonon having its wave vector in the x direction and was sufficiently large to eliminate polariton effects.

The chalcopyrite structure can be considered as a modification of the zinc-blende structure in that, as shown in Fig. 1, the unit cell consists essentially of two zinc-blende unit cells, with the A^{I} and B^{III} ions alternatively substituting on the Zn

sites.[16] The inequivalence of the cations gives rise to a displacement of the C^{VI} ion position relative to the cations, and results in the tetragonal distortion from the idealized zinc-blende structure. The tetragonal distortion of the silver compounds is sizable, with $2\text{-}c/a = 0.2103$ and $a = 5.75722$ Å for $AgGaS_2$, and $2\text{-}c/a = 0.1832$ and $a = 5.9920$ Å for $AgGaSe_2$. The copper compound has a $2\text{-}c/a = 0.0412$ and $a = 5.34741 \pm 0.00001$.[17]

The atomic weights of Cu and Ga are not very different from Zn and the tetragonal distortion of $CuGaS_2$ is correspondingly small. Thus, as discussed in Sec. IV, the vibrational spectrum of this crystal is very similar to the spectrum of ZnS when it is mapped into the chalcopyrite Brillouin zone (BZ). The larger mass of silver in $AgGaS_2$ results in a reduction of some of the phonon energies relative to $CuGaS_2$. For the silver compounds the phonon energies of the selenide are reduced by ~30% as compared to the sulfide.

The zinc-blende BZ has one-fourth the volume of the chalcopyrite BZ if the unit cell of the lattice has $c = 2a$, with a equal to the zinc-blende cell dimension. The points $\Gamma(0, 0, 0)$, $X(0, 0, \pm 2\pi/c)$, $W(\pm 2\pi/a, 0, \pm\pi/c)$, and $W(0, \pm 2\pi/b, \pm\pi/c)$ of the zinc-blende BZ ($a = b = c$) then correspond to $\Gamma(0, 0, 0)$, of the chalcopyrite BZ.[16] The zinc-blende $\vec{k} = (0, 0, 0)$, phonons belong to the Γ_{15} representation and reduce to $B_2 + E$ at Γ of D_{2d}^{12}. At the X point the (LA, TA) and (LO, TO) modes correspond to the (X_3, X_5) and (X_1, X_5) representations, and these reduce to (B_1, E) and (A_2, E) at the Γ point of the chalcopyrite BZ. The phonon modes at W do not have distinct longitudinal or transverse character. There are eight W points but symmetry arguments enable us to consider only two distinct points, which yield the 12 remaining modes.

III. EXPERIMENTAL

A. Material preparation

Single crystals were grown from the melt in evacuated sealed silica ampoules using previously described procedures.[18,19] The starting materials were 99.999% pure. The samples were oriented by x rays and faces perpendicular to the [100], [110], and [001] crystal axes were cut and polished by standard techniques. Examination of the crystal between crossed polaroids confirmed the x-ray orientation.

The color of melt-grown $AgGaS_2$ varies from light yellow to dark green. The latter color is considered to be characteristic of the stoichiometric composition with the yellow-colored crystals containing an excess of Ga.[19] A stoichiometric crystal was used for the infrared measurements. However, such crystals were found to be of relatively low optical quality and contained precipitates, cracks, and inclusions. This caused excessive scattering of the laser beam, which made the crystals unsuitable for Raman experiments. It was found that the addition of about 2-wt% Li to the starting material greatly improved the quality of the crystals. The Li-doped crystals have a light yellow color and are essentially free of precipitates. The Li^+ probably enters on the Ag^+ site, and shifts the band gap to a slightly higher energy. The polarized absorption near the band gap is shown in Fig. 2 and was obtained from several crystals of different thicknesses using a Cary spectrophotometer. For our purposes, the important feature is that the absorption well below the gap is about a factor 3 smaller than for the green-colored crystals, and that scattering is greatly reduced.

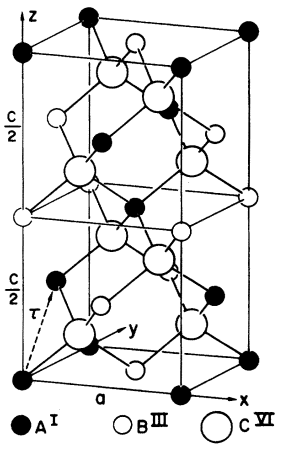

FIG. 1. Unit cell of the chalcopyrite structure for the case $c = 2a$. The relation to the zinc-blende structure is shown.

The $AgGaSe_2$ crystals had a deep-red color and are believed to be close to the stoichiometric composition. Stoichiometric $CuGaS_2$ has a yellow-green color and is difficult to obtain in the sufficiently larger crystals required for the Raman experiments. The crystals used by us had an orange-brown color, indicating a slight excess of Ga.

Our preliminary results indicated that slight deviations from stoichiometry do not significantly affect the dominant features of the Raman and infrared spectra. This justifies our use of crystals which may be slightly nonstoichiometric, but are of high optical quality.

B. Raman scattering

Raman spectra were taken using either an argon-ion laser, a krypton-ion laser, or a Coherent Radiation dye laser. All measurements were taken at room temperatures in air. Right-angle (90°), back (180°), and approximately forward (~0°) scattering geometries were used. The scattered light was dispersed using a double monochrometer and collected using a cooled S-20 photomultiplier

TABLE I. Lattice modes of the chalcopyrite structure.

$\bar{4}2m$	Symmetry	Activity	Number Optic	Number Acoustic
$A_1(\Gamma_1)$	x^2+y^2, z^2	R	1	
$A_2(\Gamma_2)$	•••	ia	2	
$B_1(\Gamma_3)$	x^2-y^2	R	3	
$B_2(\Gamma_4)$	xy; z	R, ir	3	1
$E(\Gamma_5)$	xz, y; yz, x	R, ir	6	1

and photon-counting or direct-dc-detection electronics. A typical 180° spectrum of $AgGaS_2$, using the 5145-Å argon line, is shown in Fig. 3. Crystal absorption necessitated the use of the 6471-Å krypton line for right angle and forward scattering in $CuGaS_2$. Compared to these crystals the back-scattered intensity from $AgGaSe_2$ for 5145-Å excitation was about two orders of magnitude weaker. The low intensity may well be due to the strong absorption at this energy. A somewhat better Raman spectrum of $AgGaSe_2$ was observed using the 6471-Å line which, while it is still well above the band gap, is in a region where the measured scattering intensity is somewhat stronger. The weak intensity, in addition to the fact that only the back-reflection spectrum can be observed, enabled us to identify only some of the lines.

The Raman energies are listed in Table II and the correlation with the vibrational spectrum of ZnS will be discussed in Sec. IV. With the exception of the two inactive A_2 modes, all of the modes of $CuGaS_2$, and all but one of the B_1 modes of $AgGaS_2$ were detected. In Sec. III C we show that the B_2 and E modes of $AgGaS_2$ obtained from the

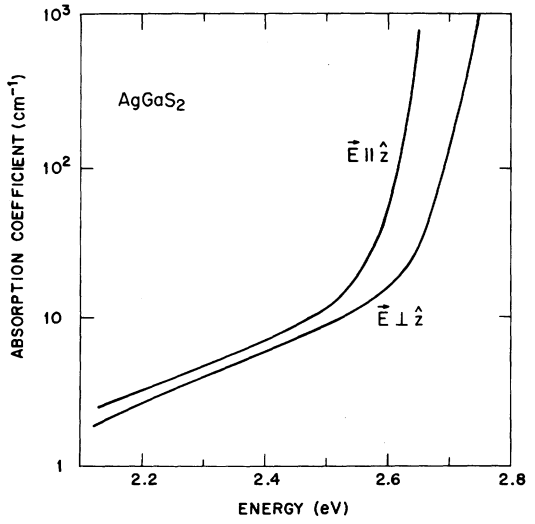

FIG. 2. Absorption of Li-doped $AgGaS_2$ at 300 °K for light polarized parallel and perpendicular to the z axis.

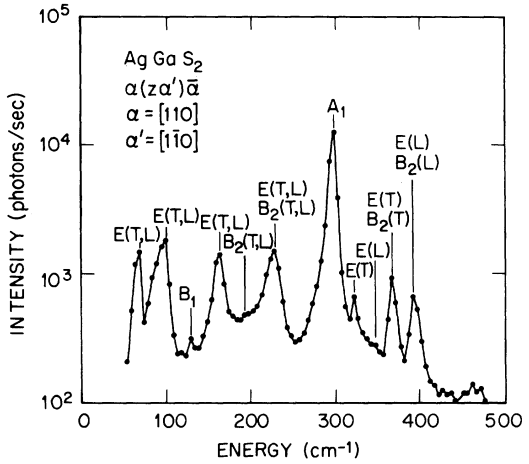

FIG. 3. Raman spectrum of $AgGaS_2$ at 300 °K for the $\alpha(z\alpha')\bar{\alpha}$ scattering geometry. For this polarization the scattering involves quasilongitudinal and quasitransverse E phonons. The B_1 and B_2 modes are forbidden and appear weakly because of the effects of birefringence and a large acceptance angle. The A_1 mode is also forbidden, but because of its large scattering intensity still appears with at least eight times the intensity of the allowed E modes.

ir data are in good agreement with the Raman measurements. Several of the $AgGaS_2$ lines agree with the work of Holah and Webb.[12] In addition, however, they identify a B_2 mode at 424 cm^{-1} as well as TO and LO components of the E mode at 464 and 473 cm^{-1} in the Raman as well as the ir spectrum. These lines are absent in our spectra, and do not appear to be associated with intrinsic $AgGaS_2$.

Some of the E-symmetry phonon energies of $CuGaS_2$ are in reasonable agreement with the incomplete infrared data of Baars and Koschel.[13] We have found weak E(T) and E(L) modes at 75 and 76 cm^{-1}, as well as E(L) modes at 95 and 167 cm^{-1} which were not observed in the infrared. The very weak infrared E(T) and E(L) modes at 387 and 399 cm^{-1} are not observed in the Raman spectrum, and agreement for the B_2 modes is also lacking. The latter may well be due to the use of $\langle\bar{1}01\rangle$ polarization in the infrared by Baars and Koschel, which results in the appearance of E as well as B_2 contributions to the reflectivity. The identification given in Table II is based on the polarization of the Raman lines, as well as the comparison with the $AgGaS_2$ data.

C. Infrared reflectivity

Reflectivity measurements in the region of 1 to 30 μm were made using the prism spectrometer described by Spitzer and Kleinman.[20] Measurements in the region of 25 to 125 μm were made using a Perkin-Elmer model 201 grating spectrom-

eter with a pumped-liquid-He-cooled bolometer as the detector. Some measurements were also made in the region of 75 to 300 μm using an RIIC Fourier spectrophotometer having a Golay cell as the detector. In each case the polarizers used were placed in such a position as to take advantage of the natural polarization of each spectrometer, while the crystal sample was positioned to give the electric field $\vec{E}$ perpendicular or parallel to the z axis.

Plots of the reflectivity for $\vec{E} \perp \hat{z}$ and $\vec{E} \parallel \hat{z}$ are shown by the points in Figs. 4 and 5, respectively. The real and imaginary parts of the dielectric constant were obtained from a Kramers-Kronig analysis of the reflectivity, and the initial estimate of the transverse- and longitudinal-mode parameters was obtained from the plots of $\mathrm{Im}(\epsilon)$ and $\mathrm{Im}(-1/\epsilon)$ shown in Figs. 4 and 5.[21] The mode frequencies ω_i were obtained from the peaks of the curves, the damping factors γ_i from the half-intensity points, and the oscillator strengths S_i from the area under the mode divided by ω_i. In terms of the classical dispersion theory the real and imaginary parts of $\epsilon_\perp$ are

$$\mathrm{Re}(\epsilon_\perp) = \epsilon_{\infty\perp} + \sum_{i=1}^{n} \frac{S_{i\perp}\omega_{i\perp}^2(\omega_{i\perp}^2 - \omega^2)}{(\omega_{i\perp}^2 - \omega^2)^2 + \omega^2\gamma_{i\perp}^2} \quad , \tag{1}$$

$$\mathrm{Im}(\epsilon_\perp) = \sum_{i=1}^{n} \frac{S_{i\perp}\omega_{i\perp}^2(\gamma_{i\perp}\omega)}{(\omega_{i\perp}^2 - \omega^2)^2 + \gamma_{i\perp}^2\omega^2} \quad , \tag{2}$$

with analogous expressions for $\epsilon_\parallel$.[22] For the $E(\perp)$ and $B_2(\parallel)$ modes n is equal to 6 and 3, respectively. The reflectivity was computed using the initial set of parameters, and then these values were varied to improve the fit to the experimental data. The parameters which yield the best fit are given in Tables III and IV, and the agreement with the reflectivity data is shown in Figs. 4 and 5.

A total of five modes were used for the oscillator fit for the $\vec{E} \perp \hat{z}$ spectrum. From the Raman data we find the missing T and L modes are at 63 and 64 cm^{-1}, and these must be quite weak in the infrared spectrum. The three very weak modes at 140, 185, and 285 cm^{-1} in the $\mathrm{Im}(\epsilon)$ spectrum are not found in the Raman spectrum, and hence do not correspond to single-phonon modes and were not included in the oscillator fit.

The three expected B_2 modes were found in the $\vec{E} \parallel \hat{z}$ spectrum. Additional weak modes were found at 128, 260, and 345 cm^{-1} in the $\mathrm{Im}(\epsilon)$ spectrum, and these modes were not included in the oscillator fit. The mode energies of the infrared-active vibrations are in good agreement with the Raman data and provides considerable confidence in the present assignment.

A test of the accuracy of the results of the Kramers-Kronig analysis is obtained by substituting the data into the sum rules

$$\epsilon_0 = \epsilon_\infty + \sum_{i=1}^{n} S_i \quad , \tag{3}$$

$$\sum_{i=1}^{n} (\omega_{iL}^2 - \omega_{iT}^2) = \sum_{i=1}^{n} \frac{S_i\omega_{iT}^2}{\epsilon_\infty} \tag{4}$$

TABLE II. Raman-active modes of $AgGaS_2$, $AgGaSe_2$, and $CuGaS_2$ at 300 °K.

Mode symmetry	Frequency (cm^{-1}) $AgGaS_2$	$AgGaSe_2$	$CuGaS_2$
E(T), E(L)	63, 64	···, 48	75, 76
E(T), E(L)	93, 96	···, 73	95, 98
B_1	118	12.5	138
E(T), E(L)	158, 160	···, 112	147, 167
B_1	179		203
B_1			243
B_2(T), B_2(L)	195, 199		259, 284
B_2(T), B_2(L)	215, 239		339, 369
E(T), E(L)	225, 230	···, 160	260, 278
A_1	295	179	312
E(T), E(L)	323, 347	···, 238	335, 352
B_2(T), B_2(L)	366, 400	···, 272	371, 402
E(T), E(L)	368, 392	···, 276	365, 387

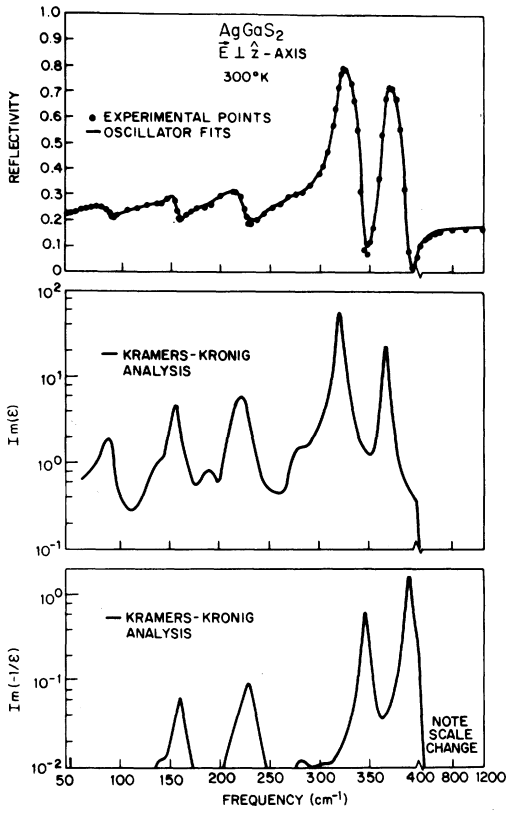

FIG. 4. Reflectivity, imaginary part of the dielectric constant, $\mathrm{Im}(\epsilon)$, and $\mathrm{Im}(-1/\epsilon)$, of $AgGaS_2$ for $\vec{E} \perp \hat{z}$ axis. The solid curve through the experimental points is the best oscillator fit to reflectivity and predicts the modes listed in Table III.

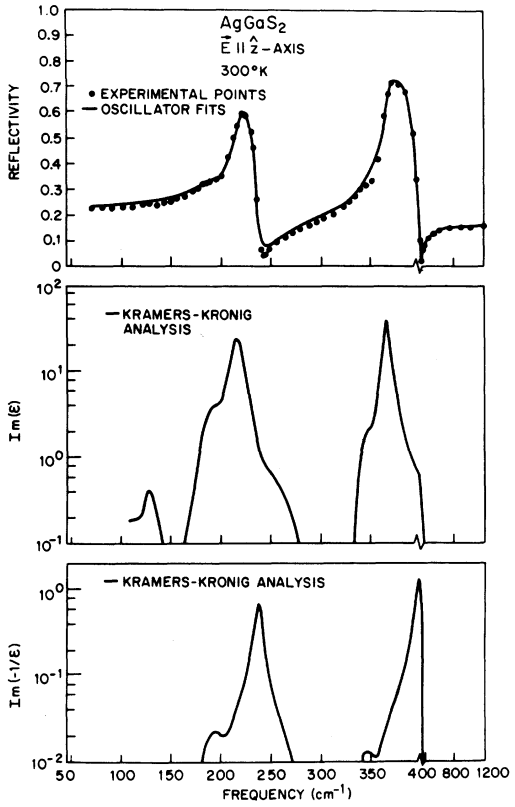

FIG. 5. Reflectivity, imaginary part of the dielectric constant, $\mathrm{Im}(\epsilon)$, and $\mathrm{Im}(-1/\epsilon)$, of $AgGaS_2$ for $\vec{E} \parallel \hat{z}$ axis. The solid curve through the experimental points is the best oscillator fit to reflectivity and predicts the modes listed in Table IV.

and the generalized Lyddane-Sachs-Teller relation

$$\prod_{i=1}^{n} (\omega_{iL}^2/\omega_{iT}^2) = \frac{\epsilon_0}{\epsilon_\infty} \quad . \tag{5}$$

The terms on each side of the equality are given in the lower part of Tables III and IV. Excellent agreement is found for the B_2 mode where all the parameters are known, but for the $\vec{E} \perp \hat{z}$ case the left side of Eq. (5) is about 5% larger than the right. In the presence of strong high-frequency modes the sum-rule relationship, Eq. (4), is not a very good test of the accuracy of the strength of the low-frequency modes. This is borne out by the good agreement which is found for the $\vec{E} \perp \hat{z}$ case even though the lowest-energy mode is neglected; but in agreement with the reflectivity data it also indicates that the strength of this mode is not anomalously large.

D. Resonant interference of the A_1 Raman mode

The $A1$ mode is the dominant feature of the Raman spectrum of $AgGaS_2$ and $CuGaS_2$. For $AgGaS_2$, at 5145 Å this line in the $y(zz)x$ scattering geometry is ~30 times stronger than the predominantly

TABLE III. Longitudinal- and transverse-optical phonon frequencies of $AgGaS_2$ for $\vec{E} \perp \hat{z}$ determined from a Kramers-Kronig analysis of Fig. 4, and the values of the parameters of the classical dispersion relations, Eqs. (1) and (2).

ω_T (cm^{-1})	ω_L	S_i	γ_i (cm^{-1})
90.0 ±1	93.0 ±1	0.26 ±0.05	13.5 ±2
157 ±1	160 ±1	0.28 ±0.05	9.7 ±1
223 ±1	230 ±1	0.40 ±0.05	15.8 ±1
323 ±1	346 ±1	1.35 ±0.05	6.78 ±0.3
368 ±1	390 ±1	0.32 ±0.02	5.34 ±0.4

$\epsilon_\infty = 5.90$; $\epsilon_0 = \epsilon_\infty + \sum S_i = 8.51 \pm 0.1$;

$\frac{\epsilon_0}{\epsilon_\infty} = 1.44$; $\prod_{i=1}^{5} \left(\frac{\omega_{iL}^2}{\omega_{iT}^2}\right) = 1.52$;

$\sum_{i=1}^{5} \frac{S_i \omega_{iT}^2}{\epsilon_\infty} = 3.61 \times 10^4$ cm^{-2}; $\sum_{i=1}^{5} (\omega_{iL}^2 - \omega_{iT}^2) = 3.67 \times 10^4$ cm^{-2}

E(L) mode at 393 cm^{-1} found in the $y(zy)x$ scattering geometry, and has ~40 times the intensity of the 922-cm^{-1} line in benzene. As shown in Fig. 3, this mode dominates the spectrum even for scattering geometries where it is forbidden unless considerable precautions against birefringence effects are taken.

The intensity of the A_1 mode decreases significantly relative to the other lines as the laser excitation energy approaches the band edge. For example, in $AgGaS_2$ the intensity is comparable to the other lines when 4579-Å (2.708 eV) argon-laser excitation is used. In Fig. 6 we have plotted the spectral dependence of this mode for the $x(zz)\bar{x}$ scattering geometry relative to the E(L) mode at 393 cm^{-1}. The E(L) mode appears in this polarization because of the effects of birefringence and the large acceptance angle of the detection system. These measurements were obtained using different

TABLE IV. Longitudinal- and transverse-optical phonon frequencies of $AgGaS_2$ for $\vec{E} \parallel \hat{z}$ determined from a Kramers-Kronig analysis of Fig. 5 and the values of the parameters of the classical dispersion relations.

ω_T (cm^{-1})	ω_L (cm^{-1})	S_i	γ_i (cm^{-1})
193 ±1	195 ±2	0.3 ±0.15	24.0
216 ±0.5	238 ±1	1.45 ±0.05	12.6 ±0.43
365 ±1	400 ±1	0.94 ±0.02	9.1 ±0.37

$\epsilon_\infty = 5.50$; $\epsilon_0 = \epsilon_\infty + \sum S_i = 8.23 \pm 0.15$;

$\frac{\epsilon_0}{\epsilon_\infty} = 1.49$; $\prod_{i=1}^{3} \left(\frac{\omega_{iL}^2}{\omega_{iT}^2}\right) = 1.49$;

$\sum_{i=1}^{3} S_i \omega_{iT}^2/\epsilon_\infty = 3.71 \times 10^4$ cm^{-2}; $\sum_{i=1}^{3} (\omega_{iL}^2 - \omega_{iT}^2) = 3.75 \times 10^4$ cm^{-2}

argon-laser lines, and by adjusting the power level and detection efficiency to be about the same for each laser line. Additional spectra were obtained using a Coherent Radiation dye laser and indicate that the relative intensity of the A_1 mode increases slightly in going from 2.0 to 2.4 eV.

By measuring the relative intensities of closely spaced Raman lines the effects due to dispersion of the absorption coefficient on the Raman intensity are largely eliminated. Using the expression for the Raman intensity in the presence of absorption given by Loudon,[23] and the absorption data in Fig. 2, the ratio of the corrected relative intensities is calculated to be at most 5% lower at 2.7 eV than shown in Fig. 6. This is less than the ±10% accuracy with which the relative intensities could be measured and justifies neglecting the absorption effect. In the vicinity of the band edge the relative intensities of the other lines are consistent with the absorption effect, and hence the intensities of these lines are relatively frequency insensitive.

Thus the A_1 mode exhibits a significant decrease in intensity as the band gap is approached, and this decrease is attributed to a resonant interference between a nonresonant and resonant term in the Raman scattering tensor. Appropriate laser frequencies were not available to follow the dispersion above 2.71 eV. However, the relative intensities of the $AgGaSe_2$ spectrum obtained using 6471- and 5145-Å excitation is qualitatively quite similar to the 4579-Å spectrum of $AgGaS_2$. It thus appears that the resonant interference does not disappear for at least ~0.7 eV above the band gap. The sharp decrease in the A_1-mode intensity at the band gap is quite different from the resonant interference in CdS, where the intensity decreases over a wider energy range and is followed by a strong resonant enhancement near the band gap.[24,25]

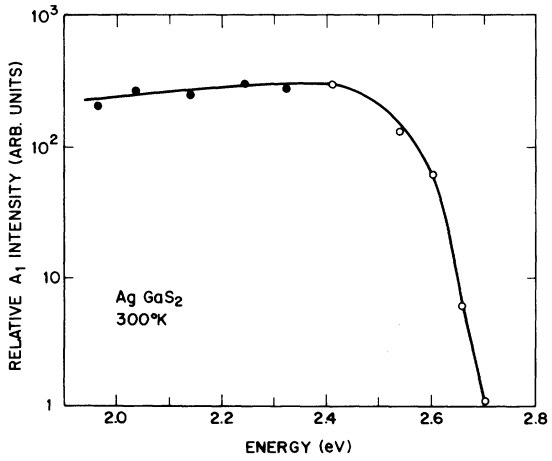

FIG. 6. Dependence of the $x(zz)\bar{x}$ scattering intensity of the 295-cm^{-1} A_1 mode of $AgGaS_2$ on laser excitation frequency. The open points were obtained using argon-laser lines and the closed points using a dye laser.

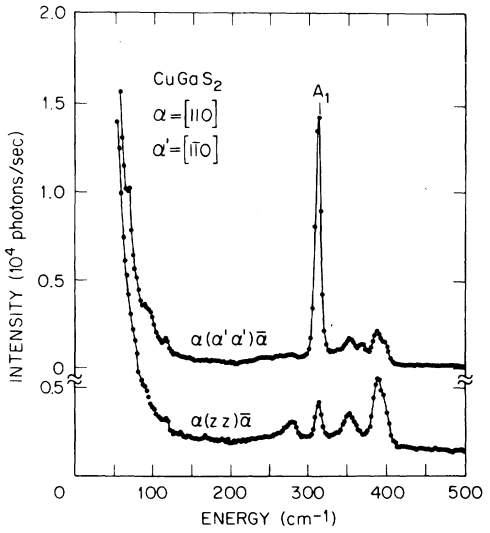

FIG. 7. Raman spectrum of $CuGaS_2$ at 300°K for 5145-Å excitation showing the effects of optical anisotropy on the A_1 intensity. The two spectra differ only in the polarization of the incident and scattered radiation.

A similar decrease in A_1 intensity has been observed for $CuGaS_2$. For both materials the interference is polarization dependent. The reduction in scattered intensity occurs at a lower laser energy when the incident and scattered light is polarized along the z axis rather than when the radiation is polarized perpendicular to this axis. The effect for $CuGaS_2$ is shown in Fig. 7 and was obtained using 5145-Å excitation, which is close to the band gap. In the lower trace the intensity of the 312-cm^{-1} A_1 line is intermediate between intensity of the 352- and 387-cm^{-1} E lines, while in the upper trace the A_1 mode has seven times the intensity of the 387-cm^{-1} line. The polarizations were changed by inserting a $\lambda/2$ plate in the incident laser beam and rotating the analyzer polaroid. This does not significantly change the laser intensity incident on the crystal or the transmission function of the spectrometer. The spectral dependence of the anisotropy of the A_1-mode intensity is found to be consistent with the optical anisotropy of the crystals.

The observation of a distinct resonance interference effect in $AgGaS_2$ and $CuGaS_2$, as well as the weak A_1-mode intensity in $AgGaSe_2$, suggests that this may be a general characteristic of chalcopyrite semiconductors. The Raman spectrum of the $A^{II}B^{IV}C_2^V$ chalcopyrite $ZnSiP_2$ was studied by Kaminow *et al.* using the He-Ne laser at 6328 Å (1.96 eV).[14] This is close to the 2.0-eV band-gap energy, and the mode intensities are roughly similar to the $AgGaS_2$ spectrum obtained

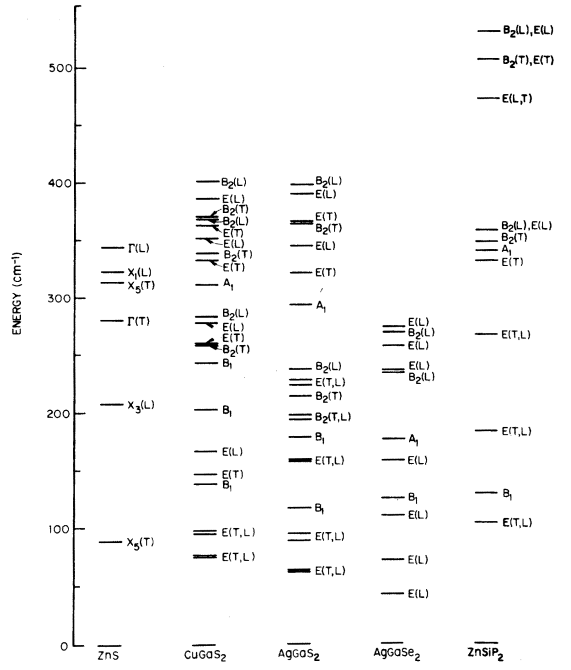

FIG. 8. Vibration-mode energies of ZnS, $CuGaS_2$, $AgGaS_2$, $AgGaSe_2$, and $ZnSiP_2$.

using 4579-Å excitation. The A_1 mode is observed to be considerably weaker than several of the other modes. Thus the limited amount of experimental data available for spectral dependence of the Raman intensities in $ZnSiP_2$ is not inconsistent with the presence of a resonance interference effect on this crystal as well.

IV. DISCUSSION

The mode energies given in Table II are compared with the Γ- and X-point energies of ZnS and the phonon energies of $ZnSiP_2$ in Fig. 8. The ZnS energies were obtained from recent neutron scattering measurements of Bergsma,[26] which differ slightly from earlier neutron and Raman data.[27,28] Neutron data for the W points is not available. However, the acoustic-W-mode energies are expected to be near the X_1(LA) and X_5(TA) energies, and the optic-mode energies will occur in the region of the Γ_{15}(LO) and Γ_{15}(TO) energies. The modes of the chalcopyrite lattice thus divide naturally into the observed three groups, corresponding approximately to the energies of the transverse- and longitudinal-acoustic X-point phonons and the optical phonons of the zinc-blende lattice.

The infrared data for $CuGaS_2$ showed that for $\vec{E} \parallel \hat{z}$ and $\vec{E} \perp \hat{z}$, a large fraction of the total oscillator strength is contained in the B_2(T) and E_2(T) modes at 331 and 259 cm^{-1}.[13] These correspond quite closely to the Γ_{15}(L) and Γ_{15}(T) vibrations of ZnS at 343 and 280 cm^{-1}. For $AgGaS_2$ we find strong B_2 modes at 216 and 365 cm^{-1}, and one strong E mode at 323 cm^{-1}. The 216 cm^{-1} mode is tentatively identified with the Γ-point phonon of the corresponding zinc-blende cell.

The ir intensities are in qualitative agreement with the point-charge model considered by Kaminow *et al.*[14] For this model the dipole moments of four E modes and one B_2 mode vanish. The cancellation of the dipole moments is not complete because the charge is somewhat distributed and modes having the same irreducible representation will interact. The "zero dipole" modes thus appear weakly in the infrared and have correspondingly small longitudinal-transverse splittings. The interaction also shifts the mode frequencies. The trend of decreasing oscillator strengths with increasing separation from the intense lines observed for both $AgGaS_2$ and $CuGaS_2$ confirms this transfer of oscillator-strength mechanism.

The atomic weights of Cu and Ag are 63.57 and 107.88, respectively, and the vibrational modes of the sulfides which involve the A^{I} atom are thus expected to have a lower energy in the silver compound. The modes involving the B^{III} and C^{VI} atoms will have nearly the same energy. The symmetry coordinates of the normal-mode vibrations have been derived by Kaminow *et al.*[14] They show that the single A_1 mode results from motion of the C^{VI} atom in the x, y plane, with the A^{I} and B^{III} atoms remaining at rest. The frequency of this mode is 5.45% lower in the Ag compound, indicating that the restoring forces acting on the S are only slightly smaller for this material. The higher A_1-mode frequency in $ZnSiP_2$ is attributed to a stronger restoring force in this compound, since the mass difference between the P and S atoms is small. Continuing to use the notation of Ref. 14, the lowest-frequency B_1 mode resembles $\nu_5(A^{\mathrm{I}})$ and $\nu_6(B^{\mathrm{III}})$ motion in phase and hence the mode frequency is

$$\nu \sim (M_{A^{\mathrm{I}}} + M_{B^{\mathrm{III}}})^{-1/2} \quad . \tag{6}$$

The calculated frequency ratio for the Ag to Cu compounds is 0.865, and this is close to the observed ratio of 0.855. The higher-energy B_1 mode involves $\nu_5(A^{\mathrm{I}})$ and $\nu_6(B^{\mathrm{III}})$ motion in antiphase and

$$\nu \sim \left[\frac{M_{A^{\mathrm{I}}} + M_{B^{\mathrm{III}}}}{M_{A^{\mathrm{I}}} M_{B^{\mathrm{III}}}} \right]^{1/2} \quad . \tag{7}$$

In this case the calculated frequency ratio is 0.885, which agrees well with the observed ratio of 0.882.

The agreement is not quite as good for all of the B_2(T) modes. The highest-frequency mode consists of $\nu_8(C^{\mathrm{VI}}) + \nu_{10}(B^{\mathrm{III}})$ motion in antiphase, which is independent of the A^{I}-atom mass. The

observed 1.5%-smaller phonon energy is consistent with this assignment. A second B_2 mode involves $\nu_8(C^{VI})+\nu_9(A^I)$ in antiphase. The calculated frequency is 0.93, and if we tentatively choose the 215- and 259-cm^{-1} B_2(T) modes the experimental frequency ratio is 0.83. The remaining mode involves $\nu_7(C^{VI})$ motion and the calculated frequency ratio is unity, but this cannot be easily explained by the experimental results. This mode has zero dipole moment in the point-charge approximation, and hence has a small L-T splitting. The B_2 modes at 195 and 199 cm^{-1} in $AgGaS_2$ fulfill the latter requirement, but such a mode has not been observed in the $CuGaS_2$ spectrum.

Two of the highest-energy E modes involve $\nu_{12}(C^{VI})+\nu_{14}(A^I)$ and $\nu_{12}(C^{VI})+\nu_{15}(B^{III})$ in antiphase motion, and the corresponding frequency ratios are 0.93 and 1.0. The former suggests that this could be the E(T) mode at 335 (Cu) and 323 (Ag) cm^{-1}, which has a frequency ratio of 0.96, and the latter the E (T) mode at 365 (Cu) and 368 (Ag) cm^{-1}. The remaining E modes have zero dipole moments in the point-charge approximation, and consist of linear comingations of $\nu_{11}(C^{VI})$, $\nu_{13}(C^{VI})$, $\nu_{16}(A^I)$, and $\nu_{17}(B^{III})$ motion. We find that the lowest- and highest-energy modes have frequency ratios of 0.84 and 0.865, respectively, indicating that these modes involve A^I as well as B^{III} or C^{VI} motion. The small frequency shifts of the two other E(T) modes indicates that the motion of these modes do not involve the A^I atoms to a significant degree.

Compared with $AgGaS_2$ the significantly smaller phonon frequencies of $AgGaSe_2$ are attributed to the larger atomic weight of Se (79.2) versus S (32.064). Thus the calculated frequency ratio of the A_1 mode based on the mass effect is 0.636. The experimental ratio is 0.607, which is somewhat smaller because the restoring force is slightly smaller in the selenide. The experimental frequency ratio for the three highest-energy E modes and the B_2 modes is 0.69 ± 0.01, which is also slightly smaller than the ratios based on the antiphase motion of A^I and C^{VI} of 0.74 and B^{III} and C^{VI} of 0.77. The measured ratios of the lowest- and next-to-lowest-energy E modes are 0.75 and 0.76, which together with the $CuGaS_2$ and $AgGaS_2$ comparison suggests that these modes involve A^I-C^{VI} and B^{III}-C^{VI} motion, respectively. The nature of the B_1 motion in the selenide is not completely understood. Its insensitivity to C^{VI} mass is explained if we associate this mode with the lowest-energy B_1 mode of $AgGaS_2$, which involves $\nu_5(A^I)+\nu_6(B^{III})$ motion in phase.

These results are in reasonable agreement with the assignments made for $ZnSiP_2$.[14] As shown in Fig. 8 the light mass of the Si yields an isolated group of high-frequency modes. Comparing $ZnSiP_2$ and $CuGaS_2$ we find the ratio of the highest-energy $E(T)$ modes is 1.42. The ratio calculated from the B^{II}-C^{VI} masses is 1.22, so that, as was already shown for the A_1 mode, the restoring forces are significantly larger in $ZnSiP_2$.

This comparison has shown that for the three materials studied there are consistent relations between many of the mode energies which are explained by the relative masses of the three ions and assuming essentially constant force constants. For $ZnSiP_2$ the mass of the Si deviates significantly from masses of the B^{III} atoms studied here, and the atomic charges are also different. In this case we find, in addition to a similar trend for the dependence on atomic weight of the atoms, that the restoring forces must be considerably larger, and this may well be related to the difference in charge.

V. SUMMARY

The Raman spectrum of the chalcopyrites $AgGaS_2$, $AgGaSe_2$, and $CuGaS_2$, as well as the infrared reflectivity spectrum of $AgGaS_2$, were measured. The mode frequencies of the latter are in good agreement with the Raman data. We find that the oscillator strengths of the infrared modes, as well as the magnitudes of the longitudinal-transverse splittings are in qualitative agreement with a point-charge model which predicts four E modes and one B mode which have vanishing dipole moments. A comparison of the phonon energies suggests that the force constants of the three crystals are about the same, and that the major contribution to the frequency shifts results from differences in the atomic masses.

The intensity of the A_1 modes of $AgGaS_2$ and $CuGaS_2$ exhibits a resonance interference effect as the laser excitation energy approaches the band gap. Like the optical absorption the interference depends on the polarization of the incident and scattered light, and occurs at a lower energy when the polarization is parallel to z than for polarization perpendicular z. It is suggested that interference may also occur in other chalcopyrite semiconductors.

ACKNOWLEDGMENTS

We wish to thank D. L. Rousseau and Frazer Williams for the use of the krypton and dye lasers. One of us (J. A. D.) is grateful to A. S. Barker, Jr. for suggesting the investigation of the $AgGaS_2$ infrared absorption. We are indebted to L. Kopf for orienting and polishing the crystals.

[1]R. Sandrock and J. Treusch, Z. Naturforsch. A 19, 844 (1964).
[2]For a general review of chalcopyrite semiconductors see J. L. Shay and J. H. Wernick, *Ternary Chalcopyrite Crystals: Growth, Electronic Structure and Applications* (Pergamon, New York, 1974).
[3]N. A. Goryunova, *Compound Diamond-Like Semiconductors* (Nauka, Moscow, 1968).
[4]D. S. Chemla, P. J. Kupecek, D. S. Robertson, and R. C. Smith, Opt. Commun. 3, 29 (1971).
[5]G. Boyd, H. Kasper, J. H. McFee, IEEE J. Quantum Electron. QE-7, 563 (1971).
[6]L. I. Berger and V. D. Prochukhan, *Ternary Diamond-Like Semiconductors* (Consultants Bureau, New York, 1969), p. 47.
[7]G. D. Boyd, H. M. Kasper, J. H. McFee, and F. G. Storz, IEEE J. Quantum Electron. QE-8, 900 (1972).
[8]B. Tell, J. L. Shay, and H. M. Kasper, Phys. Rev. B 4, 2463 (1971); J. L. Shay, B. Tell, and H. M. Kasper, Appl. Phys. Lett. 19, 366 (1971); S. Wagner, J. L. Shay, B. Tell and H. M. Kasper, Appl. Phys. Lett. 22, 351 (1973); B. Tell and H. M. Kasper, Phys. Rev. B 7, 740 (1973); J. L. Shay, P. M. Bridenbaugh, B. Tell, and H. M. Kasper, J. Lumin. 6, 140 (1973).
[9]B. Tell and H. M. Kasper, Phys. Rev. B 4, 4455 (1971).
[10]B. Tell, J. L. Shay, and H. M. Kasper, Phys. Rev. B 6, 3008 (1972).
[11]B. Tell and J. L. Shay, J. Appl. Phys. 43, 2469 (1972).
[12]G. D. Holah and J. S. Webb, in *Proceedings of the International Conference on Semiconductors, Warsaw*, 1972 (PWN-Polish Scientific Publishers, Warsaw, 1972), p. 1161.
[13]J. Baars and W. H. Koschel, Solid State Commun. 11, 1513 (1972).
[14]I. P. Kaminow, E. Buehler, and J. H. Wernick, Phys. Rev. B 2, 960 (1970).
[15]C. A. Arguello, D. L. Rousseau, and S. P. S. Porto, Phys. Rev. 181, 1351 (1969).
[16]A. S. Borshchevskii, N. A. Goryunova, F. P. Kesamanly, and D. N. Nasledov, Phys. Status Solidi 21, 9 (1967).
[17]S. C. Abrahams and J. L. Bernstein, J. Chem. Phys. 59, 1625 (1973); 59, 5415 (1973).
[18]H. M. Kasper, in *Proceedings of Fifth Materials Research Symposium, National Bureau of Standards, Gaithersburg, Md.*, 1972, U. S. Dept. of Commerce Spec. Publ. No. 364 (U. S. GPO, Washington, D. C., 1972), p. 671.
[19]H. M. Kasper, in *Proceedings of the Seventh International Symposium on the Reactivity of Solids, Bristol*, 1972 (Chapman and Hall, London, 1972), p. 46.
[20]W. G. Spitzer and D. A. Kleinman, Phys. Rev. 121, 1324 (1961).
[21]A. S. Barker, Phys. Rev. 136, A1290 (1964).
[22]F. Seitz, *Modern Theory of Solids* (McGraw-Hill, New York, 1940), p. 629.
[23]R. Loudon, J. Phys. (Paris) 26, 677 (1965).
[24]J. M. Ralston, R. L. Wadsack, and R. K. Chang, Phys. Rev. Lett. 25, 814 (1970).
[25]For a recent discussion of the dispersion of the Raman cross section in CdS with numerous references see R. H. Callender, S. S. Sussman, M. Selders, and R. K. Chang, Phys. Rev. B 7, 3788 (1973).
[26]J. Bergsma, Phys. Lett. A 32, 324 (1970).
[27]L. A. Feldkamp, G. Venkataraman, and J. S. King, Solid State Commun. 7, 1571 (1969).
[28]J. F. Vetelino, S. S. Mitra, O. Brafman, and T. C. Damen, Solid State Commun. 10, 1809 (1969).